IEEE Access
Multidisciplinary | Rapid Review | Open Access Journal

SPECIAL SECTION ON NETWORK RESOURCE MANAGEMENT IN FLYING AD HOC NETWORKS: CHALLENGES, POTENTIALS, FUTURE APPLICATIONS, AND WAYFORWARD

Received April 1, 2019, accepted June 7, 2019, date of publication June 12, 2019, date of current version June 26, 2019.

Digital Object Identifier 10.1109/ACCESS.2019.2922211

Robust RFID Based 6-DoF Localization for Unmanned Aerial Vehicles

JIAN ZHANG[1], XIANGYU WANG[1,2], ZHITAO YU[1,2], YIBO LYU[1], SHIWEN MAO[2], (Fellow, IEEE), SENTHILKUMAR CG PERIASWAMY[1], JUSTIN PATTON[1], XUYU WANG[3], (Student Member, IEEE)

[1]The RFID Lab, Auburn University, Auburn, AL 36849, USA
[2]Department of Electrical and Computer Engineering, Auburn University, Auburn, AL 36849-5201, USA
[3]Department of Computer Science, California State University, Sacramento, CA 95819-6021, USA

Corresponding author: Shiwen Mao (smao@ieee.org)

This work was supported in part by U.S. NSF under Grant CNS-1702957, and in part by the RFID Lab and the Wireless Engineering Research and Education Center (WEREC) at Auburn University.

ABSTRACT Although Unmanned Aerial Vehicles (UAV) are usually deploy outdoors, there is increasing interest in applying UAVs for indoor applications. It is a highly attractive and challenging task to precisely localize a UAV in an indoor environment where Global Positioning System (GPS) service is absent. In this paper, we present RFUAV, a Radio-frequency Identification (RFID) enhanced UAV system that provides a precise 6 degrees of freedom (6-DoF) pose for UAVs. With RFUAV, three or more ultra high frequency (UHF) RFID tags are attached to the UAV and are interrogated by a Commercial Off-The-Shelf (COTS) RFID reader with multiple antennas. Based on phase measurements of the RFID tag responses, the RFID tracker of RFUAV, a Bayesian filter-based algorithm, was employed to track the position of the tags in a global coordinate system. The pose estimator of RFUAV computes the 6-DoF pose of the UAV from tag positions. We tested the performance of RFUAV in a representative, structure-rich, indoor environment, where 0.04 m position error and 2.5 degrees orientation error were achieved.

INDEX TERMS Radio-frequency identification (RFID), six degrees of freedom (6-DoF), indoor localization, unmanned aerial vehicle (UAV).

I. INTRODUCTION

The last decade witnessed a tremendous growth of interest in unmanned aerial vehicles (UAV) [1]. Thanks to its outstanding maneuverability, small size, and low cost, UAVs have been widely adopted for surveillance, entertainment, search and rescue, inspection, and maintenance applications. These applications occur mostly in outdoor environments with existing navigation systems that rely on inertial sensors and Global Positioning System (GPS). Due to the low positioning resolution and the absence of GPS signal in an indoor environment (i.e.,warehouses, retail stores, etc.), most existing UAVs are infeasible for operation indoors. Consequently, recent research has investigated the problem of UAV indoor localization. The most popular indoor UAV localization methods can be categorized by measurement into three groups: vision-/laser-based, inertial navigation system (INS)-based, and wireless signals-based solutions.

The associate editor coordinating the review of this manuscript and approving it for publication was Omer Chughtai.

The vision-based solutions are proposed to exploit the visual information provided by one or two cameras [2]–[6] for UAV indoor localization and navigation. Most of the vision-based solutions are leveraged with simultaneous localization and mapping (SLAM) technologies and use an Iterative Closest Point (ICP) algorithm to achieve real-time indoor localization. One of the first real-time, monocular SLAM methods based on nonlinear filtering was proposed by Chiuso *et al.* [7]. Most laser-based approaches employ a similar architecture to tackle the indoor UAV location. Instead of visual signals, they rely on laser beams to estimate the location of the UAV. Nevertheless, the SLAM technologies are easily challenged with issues related to the use and collection of feature points and their inability to provide stable and highly accurate localization in a complex indoor environment.

The INS is a navigation system that uses the Inertial Measurement Unit (IMU) to track the speed, position, and orientation of a device. With the development of Microelectromechanical systems (MEMS) technology, researchers can equip a small and low-cost IMU on a UAV, while many

modern mini-UAVs have integrated the IMU internally. However, because of unavoidable, inherent hardware error and the error accumulated during the drift, accuracy will decrease after the UAV has been flying for a certain period of time [8].

With the astonishing growth of wireless systems and applications, many researches now focus on RF based indoor localization [9]–[19]. The basic concepts of indoor wireless localization are suitable for UAV. Up to now, many systems based on received signal strength indicator (RSSI) and Ultra-wideband (UWB) were designed for localizing UAV in GPS-denied indoor environments. RSSI is a cheap and efficient way to measure distance and position, but its accuracy is unsatisfactory. Stojkoska *et al.* [20] presented an algorithm based on measurements of the distance between a UAV and the existing infrastructure consisting of Wi-Fi Access Points (APs). With known locations of APs, a UAV is deployed to collect RSSI from the Wi-Fi APs during flight, transform these measurements into distances, and draw the flight trajectory with 33 points. The ultra large bandwidth of UWB technology enables highly precise time measurements using Time Difference of Arrival (TDOA). Tiemann *et al.* proposed a cooperative UWB positioning system that enabled autonomous flying of a UAV [21]. This state-of-the-art UAV indoor localization work integrated UWB and INS technology. For example, Li *et al.* utilized UWB, INS, and 3D laser scanner data fusion, which is based on a Kalman filter, to achieve precise UAV indoor localization [22].

Meanwhile, radio-frequency identification (RFID) technology, especially the passive UHF RFID, has been widely deployed in retail environments [23]. RFID was developed as a cost-effective wireless technique for item serialization and has been widely recognized as a promising solution for indoor localization [24]–[28]. Due to lightweight and low-cost RFID tags, the RFID technology offers a promising method for UAV indoor localization. Choi *et al.* first proposed the concept of using passive RFID tags for indoor UAV localization in [29]. However, they only demonstrated their concept and design of the system but lacked experimental validation. Recently, RFID technology was used in 3D reconstruction. For example, Bu *et al.* presented a new theory based on the phase difference of RFID tags for 3D reconstruction of standard cubes [30]. Most existing RFID-based 3D reconstruction methods adopt an architecture of finding optimized results among multiple potential poses [30]–[32], which limits their applicability for UAV indoor localization, where six degrees of freedom (6-DoF) poses are needed in real-time.

In this paper, we present the **RFUAV** – a low-cost **RF**ID based system to localize a **UAV** and enable it to autonomously navigate in complex indoor environments, such as warehouses, retail stores, hazmat storage facilities, and factories. Usually, such environments are crowded with racks, shelves, furniture, and other items of various sizes and layouts. With the increase in popularity of UAVs, there has come an increased concern with UAVs and public safety, leading to a compelling need for accurately locate an UAV in such 3-D indoor space [33], [34]. The proposed RFUAV will be deployed in an indoor environment to maintain the UAV's precise positioning, prevent collisions with other objects, and, hence, reduce the safety risks while flying in target environments. Our idea for RFUAV was motivated by existing RFID based 3D reconstruction work [27]. However, the proposed method can provide precise 6-DoF poses, including both position and orientation in a 3D space, in real-time. In RFUAV, N ($N \geq 3$) UHF passive RFID tags are attached to a UAV, the position of each tag against the built-in coordinate of the UAV is measured first. This position is denoted as a *local* position. Then, a COTS (Commercial Off-The-Shelf) RFID reader with multiple antennas is deployed to collect observation of the tags. Based on the phase measurement of each RFID tag's response at multiple antennas, we can precisely track the position of the tags in the global coordinates of the 3D space. We denote this position as a *global* position. With the known local position of each tag and the global position of the N tags, the 6-DoF pose of the UAV is determined. Note that the reader and antennas are installed on the ground and powered from the target environment, while only the passive UHF RFID tags are attached to the UAV in the proposed scheme. Thus, the RFUAV system does not incur any extra power consumption to the UAV. Furthermore, the RFID infrastructure is already deployed in most of our target environments and the proposed system can be seamlessly integrated without much extra financial investment.

The main contributions of this work are summarized as follows:

1) We developed a real-time RFID tag tracing system that incorporates a Bayesian filter [35]. Based on the phase measurements of RFID responses from a COTS reader, the tag tracker can track the motion of multiple UHF RFID tags simultaneously.
2) We propose a real-time UAV pose estimator. Based on the positions of the attached tags, the pose estimator can compute precise 6-DoF poses for the UAV in a 3D space with a singular value decomposition method.
3) We tested the RFUAV system with COTS RFID tags and reader and demonstrate its performance in a representative indoor environment. Experimental results demonstrate that RFUAV can achieve precise poses with only 0.04m error in position and 2° error in orientation. Such performance enables a UAV to autonomously navigate in an indoor environment.

The remainder of this paper is organized as follows. The preliminaries are discussed in Section II. We present the proposed approach and the analysis of the RFUAV system in Section III and our experimental study in Section IV. Section V concludes this paper.

II. PRELIMINARIES

A. PHASE MODEL FOR AN UHF RFID SYSTEM

To interrogate RFID tags, continuous-wave (CW) signals are transmitted by an RFID reader. The phase value of a tag response measured by the reader describes the phase difference between the transmitted signal and the corresponding

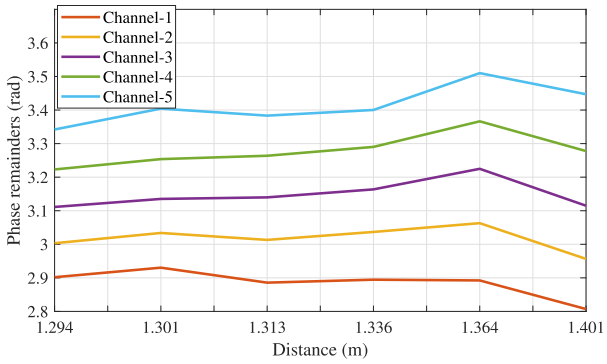

FIGURE 1. Phase remainders ($\theta' + \theta_{noise}$) at 6 sampling positions.

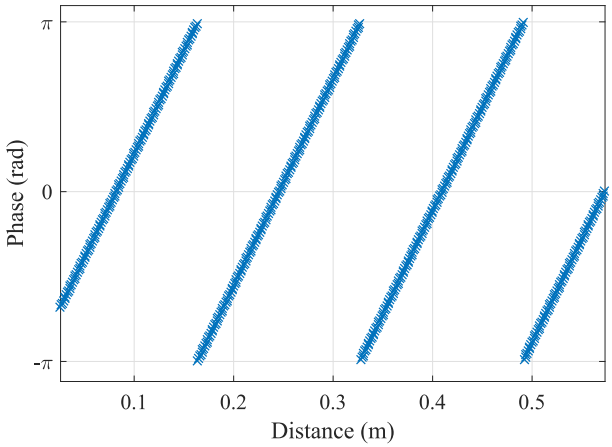

FIGURE 2. The linear relationship between the phase of RFID tag response and tag-antenna distance on a given channel.

received signal, which ranges from $-\pi$ to π. Nowadays phase values can be read by many commercial RFID readers, such as Impinj R420 [36] and Zebra FX7500 [37]. Specifically, the phase value depends on the spatial distance between the tag and the reader's antenna. Letting d denote the tag-antenna distance, the measured phase value θ can be expressed as:

$$\theta = \left(2\pi\left(\frac{2d}{\lambda}\right) + \theta' + \theta_{noise}\right) \bmod 2\pi, \tag{1}$$

where λ is the wavelength of the channel, *mod* represents the modulo operation, and θ_{noise} is the phase offset caused by thermal noise and is a normal random variable. θ' is the phase offset caused by the reader's transmit/receive circuits and the tag circuits, which is expressed as:

$$\theta' = \theta_T + \theta_R + \theta_{TAG}, \tag{2}$$

where θ_T, θ_R, θ_{TAG} are the RF phase rotation caused by the reader's transmit circuits, the reader's receive circuits, and the tag's reflection characteristics, respectively.

Even though θ' is unknown, it dependents on the given hardware and is quite stable over time. We first conducted a benchmark experiment, as follows, to demonstrate that the phase offset θ' is stable while the tag moves throughout the environment. As the tag moves within the detectable range of the antenna, the measurement θ and the associated distance d to the antenna are recorded at several positions. According to (1), the theoretical phase is calculated as $\theta_T = 2\pi\left(\frac{2d}{\lambda}\right)$. The phase remainder is determined by $\theta' + \theta_{noise} = unwrap(\theta) - \theta_T$, where $unwrap(\cdot)$ adjusts the radian phases by adding multiple $\pm 2\pi$ to remove the phase discontinuities introduced by the round operation, while the distance between the tag and the antenna continuously increases Fig. 1 shows the experimental results of phase remainders that are measured at 6 positions when the tag moves. It shows that the phase remainders of 5 channels at the 6 locations are quite stable. The maximum phase remainder change occurs on channel-5, which is 0.15 rad. Considering that θ_{noise} is about 0.1 rad, θ' remains quite stable as the tag moves. Therefore, θ' could be easily removed from the phase observation. As shown in Fig. 2, the measured phase value repeats from $-\pi$ to π with a period of a half wavelength. Within a half wavelength and for a given channel, the phase value exhibits a linear relationship with the distance between the tag and the reader's antenna.

B. COORDINATES OF THE UAV

In general, the UAV is flying in a three-dimensional environment which has six degrees of freedom (6-DoF). Three translational degrees of freedom (DoFs) represent the *position* and three rotational DoFs represent the *orientation*. A pose of a UAV is depicted by the combination of position and orientation. A common means to describe the pose of a UAV is to attach it to a frame coordinate system. After a frame coordinate system is defined, the pose can be described by the origin and orientations of the axes of the frame. A pose $\mathbf{P}$ referring to given frame coordinates $\mathcal{A}$ can be denoted as:

$$\mathbf{P} = [\mathbf{T}, \mathbf{R}]^T, \tag{3}$$

where $\mathbf{T}$ and $\mathbf{R}$ are the position and orientation against frame $\mathcal{A}$, respectively, and $(\cdot)^T$ is the transpose operation.

In our proposed RFUAV system, two frame coordinates are created to depict the UAV position. The first one is called the global frame coordinate system, which is denoted by g, representing the experimental environment coordinates. The second one is the UAV's built-in frame coordinate system, which is denoted by c, representing the UAV reference coordinate system. To translate a position from the UAV's built-in coordinates to the global coordinates, a rigid transformation, ${}^g_c\mathbf{T}$, is calculated and consists of a translation matrix, $\mathbf{T}$, and a rotation matrix, $\mathbf{R}$. Here, $\mathbf{T}$ and $\mathbf{R}$ are the position and orientation of the UAV against the global coordinates, which are given in (3). When we obtain a position $\bar{\mathbf{l}}_n = (\bar{x}_n, \bar{y}_n, \bar{z}_n)^T$ in the UAV's built-in coordinate system, the corresponding global position $\mathbf{l}_n = (x_n, y_n, z_n)^T$ can be derived by:

$$\mathbf{l}_n = \mathbf{R} \cdot \bar{\mathbf{l}}_n + \mathbf{T}. \tag{4}$$

The translation matrix $\mathbf{T}$ describes the position shift of the UAV's built-in frame c with reference to the global frame g.

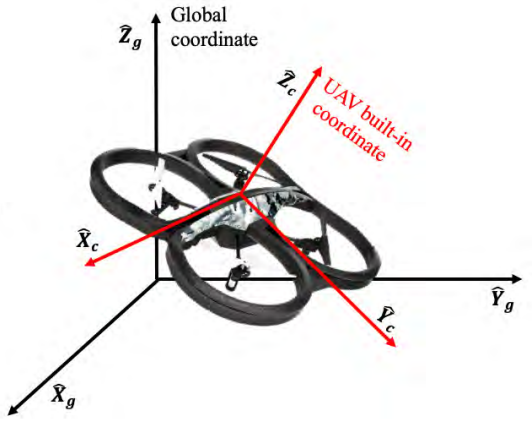

FIGURE 3. The global coordinate system and the UAV's built-in local coordinate system.

Let $[o_x^g\ o_y^g,\ o_z^g]$ and $[o_x^c,\ o_y^c,\ o_z^c]$ be the origin point positions of frame g and c, respectively. Then $\mathbf{T}$ can be expressed as:

$$\mathbf{T} = [o_x^g - o_x^c, o_y^g - o_y^c, o_z^g - o_z^c]^T. \tag{5}$$

Rotation matrix $\mathbf{R}$ describes the relative relationship of orientations between the two frames. The orientation of the UAV's built-in frame c with a reference to the global frame g is expressed by $\mathbf{R}$ as:

$$\mathbf{R} = \begin{bmatrix} \hat{X}_c \cdot \hat{X}_g & \hat{Y}_c \cdot \hat{X}_g & \hat{Z}_c \cdot \hat{X}_g \\ \hat{X}_c \cdot \hat{Y}_g & \hat{Y}_c \cdot \hat{Y}_g & \hat{Z}_c \cdot \hat{Y}_g \\ \hat{X}_c \cdot \hat{Z}_g & \hat{Y}_c \cdot \hat{Z}_g & \hat{Z}_c \cdot \hat{Z}_g \end{bmatrix}, \tag{6}$$

where $\hat{X}_c$, $\hat{Y}_c$, and $\hat{Z}_c$ are the unit vectors of the axes of the UAV's built-in coordinate frame, and $\hat{X}_g$, $\hat{Y}_g$, and $\hat{Z}_g$ are the unit vectors of the axes of the global coordinate system. The relationship between the two coordinate systems is illustrated in Fig. 3.

III. THE PROPOSED APPROACH AND ANALYSIS

The RFUAV system is a low-cost, RFID-based system that enables a UAV to autonomously navigate in a complex indoor environment. This is achieved by providing precise 6-DoF poses of the UAV in a 3D space, which includes both position and orientation. Specifically, we attach N ($N \geq 3$) UHF passive RFID tags to a UAV. Through tracking the RFID tags with phase measurements, we can estimate the 6-DoF pose of the UAV. In this section, we introduce the system model, architecture, and analysis of RFUAV.

A. SYSTEM ARCHITECTURE

The architecture of RFUAV is illustrated in Fig. 4. The proposed system consists of two main components.

- **RFID tracker**: Based on phase measurements from the reader, a Bayesian filter is used to track the position of the tags against the global coordinates in a 3D space.
- **Pose estimator**: After the RFID tracker provides the global position of N ($N \geq 3$) tags, with the known local position of the tags compared to the UAV's built-in coordinates, the pose of the UAV can be estimated by an SVD-based algorithm.

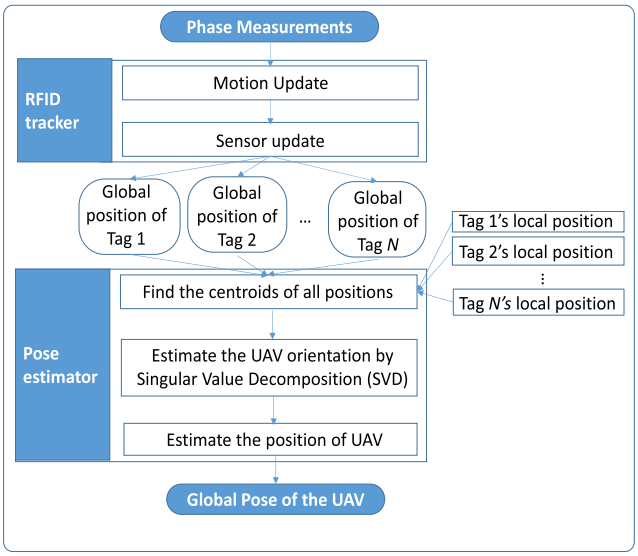

FIGURE 4. The system architecture of RFUAV, including the RFID tracker and pose estimator.

B. RFID TRACKER

In the RFUAV system, an RFID reader with M antennas is deployed to obtain phase measurements from responses of the attached tags. The positions of all antennas are already known. Hereafter, we use h_m^g to denote the position of the mth antenna in the global coordinate.

1) BAYESIAN FILTER UPDATES FOR TAG TRACKING

The RFID tracker utilizes a Bayesian filter to estimate (or track) tag locations. The Bayesian filter addresses the problem of estimating belief over the hypothetical posterior state l of a dynamic system from sensor observations. Here, state l denotes the location of the tag in the global coordinate system. The Bayesian filter recursively updates the belief $bel\ (l_t)$, which denotes the probability of the system in state l at time t. The $bel\ (l_t)$ is calculated from control u_t, observation z_t, and prior belief $bel\ (l_{t-1})$ at time $t-1$, which is calculated previously.

There are two essential steps for the updating cycle of a typical Bayesian filter. The first step is called control update or prediction, which is given by:

$$\overline{bel}\ (l_t) = \int P\ (l_t | u_t, l_{t-1})\ bel\ (l_{t-1})\ dl_{t-1}, \tag{7}$$

where $P\ (l_t | u_t, l_{t-1})$ is a motion model and provides the probability for a tag to move from state l_{t-1} to l_t after control u_t is applied, and $\overline{bel}\ (l_t)$ denotes the state probability distribution of the tag after control u_t is applied. We deploy a constant speed mobility model for the RFID tracker, i.e., we assume that in a very short time interval, the speed of a tag will

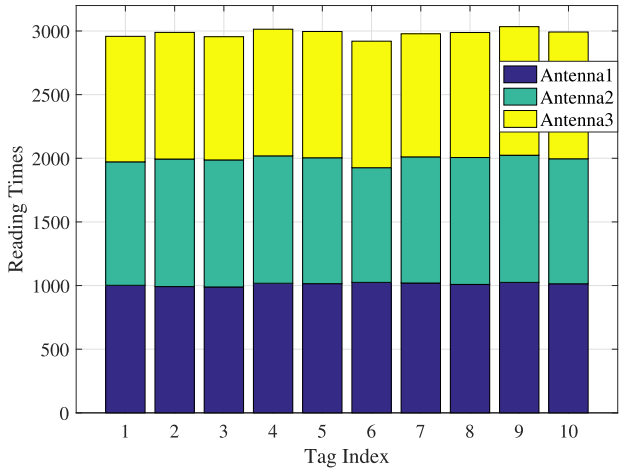

FIGURE 5. Reading occurrences of 10 tags by 3 antennas in a period of 60 seconds.

remain constant. We do not assume that the tag moves at a constant velocity over all time, but rather that it maintains an average speed, u_t, with an undetermined and negligible amount of acceleration within a short time frame. Its movement can be described mathematically by a Gaussian distribution as [35]:

$$P(l_t|u_t, l_{t-1}) = \frac{1}{\sqrt{2\pi}\xi}\int_0^{\Delta t} e^{-\frac{(l_t-(l_{t-1}+u_t\cdot\tau))^2}{2\xi^2}} d\tau, \quad (8)$$

where u_t is the speed of the item at time t (i.e., the control), Δt is the time interval between $t-1$ and t, and ξ^2 is the variance to model the movement of the item satisfying a typical Gaussian distribution.

A commercial RFID reader can interrogate tags at a rate of about 500Hz. To demonstrate this, we provide an experimental setting of a reader connected with 3 antennas to read 10 tags in an environment where there are hundreds of tags. Fig. 5 shows how many times each of the 10 tags were read by three antennas within 60 seconds. This benchmark experiment was conducted in a mock apparel store, where hundreds of RFID tags were deployed in the environment. During the experiment, we enabled the filter function, which is available for most COTS readers, of the reader to only interrogate the 10 given tags. Each tag was read for about 3000 times (1000 times per antenna) in a period of 60 seconds. Thus, each tag can be interrogated by the reader for about 50 times per second. Considering N ($10 > N \geq 3$) tags will be attached to the UAV, the practical reading frequency should be larger than 50Hz. Thus, the interval of two continuous observations of the tag is about $10 \sim 20$ milliseconds. In such a short period, our constant speed model in (8) should be suitable, since for indoor deployment of UAVs, the speed is usually lower than that in outdoor applications. Therefore, for practical applications, we can program the filter function to ensure the assumption of (8) be maintained.

The second step is measurement update, which is given by:

$$bel(l_t) = \eta \cdot \overline{bel}(l_t) \cdot P(z_t|l_t). \quad (9)$$

In (9), η is a constant that helps to normalize the sum of all $bel(l_t)$ to 1, and $P(z_t|l_t)$ is called the *observation model*. In the RFID tracker, M reader antennas are deployed. Therefore, $P(z_t \mid l_t)$ is given by:

$$P(z_t|l_t) = \prod_{m=1}^{M} P\left(z_t|l_t, h_m^g\right). \quad (10)$$

We can thus rewrite (9) as:

$$bel(l_t) = \prod_{m=1}^{M} \eta \cdot \overline{bel}(l_t) \cdot P\left(z_t|l_t, h_m^g\right). \quad (11)$$

where $P(z_t|l_t, h_m^g)$ is the observation model for the mth antenna, which provides the probability for the tag to be located in position l_t, and the measurement of z_t is observed by the mth antenna that is in a known position h_m^g. More details of the observation model are given in the next subsection.

2) THE OBSERVATION MODEL OF RFID PHASE MEASUREMENT

The relationship of the RF phase shift between the sent and received signals is given by (1) and (2). The experimental results in Fig. 1 show that θ_T, θ_R, θ_{TAG} are relatively constant when the reader antenna, the RFID tag, and the radio frequency are fixed. When we consider the RF phase for the same antenna, the same RFID tag, and under the same RF frequency, and ignore θ_{noise},[1] (1) can be rewritten as:

$$\theta = \left(2\pi \cdot \left(\frac{2d}{\lambda}\right) + \theta'\right) \bmod 2\pi. \quad (12)$$

Assume a reader antenna is set in position h_m^g, a tag is in position l_{t-1}, and the RF phase θ_1 for the tag is observed. When the tag moves to position l_t, it generates an RF phase θ_2 under the same frequency. The differential RF phase between these two positions satisfies the following relationship.

$$\Delta\theta_{12} = (\theta_1 - \theta_2) \bmod 2\pi \quad (13)$$

$$\Delta\theta_{12} = \left(\left(2\pi\left(\frac{2\left|l_{t-1}, h_m^g\right|}{\lambda}\right) + \theta'\right) \bmod 2\pi - \left(2\pi\left(\frac{2\left|l_t, h_m^g\right|}{\lambda}\right) + \theta'\right) \bmod 2\pi\right) \bmod 2\pi \quad (14)$$

$$\Delta\theta_{12} = \left(\frac{4\pi}{\lambda} \cdot \left(\left|l_{t-1}, h_m^g\right| - \left|l_t, h_m^g\right|\right)\right) \bmod 2\pi, \quad (15)$$

where $|\cdot,\cdot|$ measures the Euclidean distance between two positions. Equation (15) shows that the differential RF phase, under the same frequency, the same antenna, and the same RFID tag, can be determined by the difference of distances when the tag moves from one position to another. In other words, $\Delta\theta_{12}$ is not affected by the constant phase offset θ' and is only related to the distance between the two positions. Hereafter, we assume that all the RF phases are measured by

[1] The modeling of θ_{noise} will be introduced later.

the same reader antenna for the same RFID tag at the same RF frequency. The antenna of the RFID reader is stationary in a known position h_m^g. The tag will be located in a series of positions denoted as $\{l_1, l_2, \ldots, l_t\}$, and the corresponding phase shifts for these positions are $\{\theta_1, \theta_2, \ldots, \theta_t\}$. It follows that

$$\begin{cases} \left|l_i, h_m^g\right| - \left|l_j, h_m^g\right| = \dfrac{\lambda}{4\pi} \cdot \Delta\theta_{ij} + n \cdot \dfrac{\lambda}{2} \\ \Delta\theta_{ij} = (\theta_i - \theta_j) \bmod 2\pi, \end{cases}$$
$$n = \{1, 2, \ldots\}, \quad i, j \epsilon \{1, 2, \ldots, t\} \text{ and } i \neq j. \tag{16}$$

We next update the observation model $P(z_t | l_t, h_m^g)$ by (16), which gives the probability that a tag moves from l_t to l_{t-1} to achieve the differential RF phase shift $\Delta\theta_{t,t-1}$. The model of differential RF phase is given by:

$$P\left(\Delta\theta_{t,t-1} \left| l_{t-1}, l_t, h_m^g \right.\right) = \begin{cases} 1, & \text{if (16) is satisfied} \\ 0, & \text{otherwise.} \end{cases} \tag{17}$$

The RF phase is measured by the reader antenna, and usually it is distorted by thermal noise, denoted by θ_{noise} in (1). Experiments reveal that θ_{noise} satisfies a typical Gaussian distribution. Therefore, the RF phase containing this random error can be modeled as $\theta \sim \mathcal{N}(\mu, \delta^2)$, where μ is the mean of the RF phase without thermal noise and δ^2 is the variance. It follows that the phase difference, as the difference of two Gaussian random variables, is also Gaussian as $\Delta\theta_{ij} \sim \mathcal{N}(\mu_i - \mu_j, 2\delta^2)$. Incorporating the thermal noise to (17), we have

$$P\left(\Delta\theta_{t,t-1} | l_{t-1}, l_t, h_m^g\right) = \frac{1}{\sqrt{2\pi}\delta} \int_0^{\Delta\theta_{t,t-1}} e^{-\frac{(y-(\mu_t-\mu_{t-1}))^2}{2\delta^2}} dy, \tag{18}$$

where

$$\mu_t - \mu_{t-1} = \left(\frac{2\left|l_t, h_m^g\right|}{\lambda} - \frac{2\left|l_{t-1}, h_m^g\right|}{\lambda} \right) \bmod 2\pi. \tag{19}$$

To consider thermal noise when estimating the location of RFID tags by (11), we can use (18) instead of (17).

C. POSE ESTIMATOR

The RFID tracker provides the tag position in the global coordinate system. We use $\mathbf{l}_n^t = (x_n^t, y_n^t, z_n^t)^T$ to denote the global position of tag n at time t. With the UAV be located at $\mathbf{T}_t$, with orientation $\mathbf{R}_t$ in the given global coordinate system, while $\mathbf{T}_t$ and $\mathbf{R}_t$ together provide the pose of the UAV at time t. The position of each attached tag in the UAV built-in coordinate is known and fixed. We indicate this local position for the nth tag as $\bar{\mathbf{l}}_n = (\bar{x}_n, \bar{y}_n, \bar{z}_n)^T$. The relationship between local and global positions is given by (4), which can be rewritten as:

$$\mathbf{l}_n^t = \mathbf{R}_t \cdot \bar{\mathbf{l}}_n + \mathbf{T}_t, \tag{20}$$

where $\mathbf{R}_t$ and $\mathbf{T}_t$ are the orientation and position of the UAV in the global coordinate system at time t, respectively; and $\mathbf{l}_n^t$ and $\bar{\mathbf{l}}_n$ are the locations of the nth tag in the global coordinate system and the UAV built-in coordinate system, respectively.

When the RFID tracker localizes three or more tags simultaneously, we can use (20) to obtain an optimal transformation ${}_c^g\mathbf{T}_t$, which consists of $\mathbf{R}_t$ and $\mathbf{T}_t$. The method to solve (20) will be introduced later in this section. In practice, the RFID reader cannot query multiple tags simultaneously. However, we can assume the three consecutive queries happen at the same time. This assumption is reasonable for most indoor UAV applications. Unlike the scenario of moving rigid body localization discussed in [49], the UAV usually moves at a much lower speed (e.g., 1 m/s) in an indoor environment. As discussed previously, the current RFID reader can conduct 500 queries per second, which is only 2 ms per query. In such a short time period the displacement of the UAV is only about several millimeters (e.g., 2 mm when a UAV moves at 1 m/s) and can be ignored. Therefore, when the N tags are located by the RFID tracker, it follows (20) that

$$\begin{cases} \mathbf{l}_1^t = \mathbf{R}_t \cdot \bar{\mathbf{l}}_1 + \mathbf{T}_t \\ \mathbf{l}_2^t = \mathbf{R}_t \cdot \bar{\mathbf{l}}_2 + \mathbf{T}_t \\ \quad \ldots \\ \mathbf{l}_N^t = \mathbf{R}_t \cdot \bar{\mathbf{l}}_N + \mathbf{T}_t, \end{cases} \tag{21}$$

where $\mathbf{l}_1^t$, $\mathbf{l}_2^t$, and $\mathbf{l}_3^t$ are the global positions for tags 1, 2, and 3, respectively; and $\bar{\mathbf{l}}_1$, $\bar{\mathbf{l}}_2$, and $\bar{\mathbf{l}}_3$ are the local positions (measured in the built-in coordinate of the UAV) for tags 1, 2, and 3, respectively. The goal is to find the optimal transform ${}_c^g\mathbf{T}_t$, which includes rotation $\mathbf{R}_t$ and translation $\mathbf{T}_t$, between two sets of corresponding 3D data points. The task can be formulated as a least squares minimization problem as:

$$\min_{\{\mathbf{R}_t, \mathbf{T}_t\}} \sum_{i=1}^{N} ||\mathbf{l}_i^t - (\mathbf{R}_t \cdot \bar{\mathbf{l}}_i + \mathbf{T}_t)||, \tag{22}$$

where $||\cdot||$ is the norm of a vector. Determining the rotation and translation relationship between two sets of data points at different coordinates is a typical problem in pattern analysis [47], [48]. Based on the method introduced in [47], the proposed pose estimator is developed to find the optimal ${}_c^g\mathbf{T}_t$ with the following procedure:

1. Find the centroids of all the positions in both the global coordinate system and the UAV's built-in coordinate system.
2. Use the centroids as the new origin of the two coordinate systems, and transforming the positions into these two coordinates. Then based on these transformed positions to find the optimal rotation $\mathbf{R}_t$ with the singular value decomposition (SVD) method.
3. Solve for the translation $\mathbf{T}_t$ using rotation $\mathbf{R}_t$.

In Step 1, the centroids are computed as:

$$\begin{cases} \mathbf{O}_g = \dfrac{1}{N} \sum_{i=1}^{N} \mathbf{l}_n^t \\ \mathbf{O}_c = \dfrac{1}{N} \sum_{i=1}^{N} \bar{\mathbf{l}}_n, \end{cases} \tag{23}$$

where $\mathbf{O}_g$ and $\mathbf{O}_c$ are the centroids of all the positions in the global and the UAV's built-in coordinate systems, respectively.

In Step 2, we use $\mathbf{O}_g$ and $\mathbf{O}_c$ as new origins to shift the global and UAV's built-in coordinates to create two new coordinate systems, which are called the *shifted* global and *shifted* UAV's built-in coordinate systems, respectively. The positions in these two coordinates, which are denoted as $\bar{\mathbf{P}}_g^i$ and $\bar{\mathbf{P}}_c^i$, are given by:

$$\begin{cases} \bar{\mathbf{P}}_g^i = \mathbf{l}_i^t - \mathbf{O}_g \\ \bar{\mathbf{P}}_c^i = \bar{\mathbf{l}}_i - \mathbf{O}_c, \end{cases} \quad \text{for } i \in [1, 2, \ldots, N]. \tag{24}$$

We then apply the SVD method to find the optimal rotation between the two sets of positions in the shifted global and shifted UAV built-in coordinate systems. First, we create a matrix $\mathbf{H}$, which is given by:

$$\mathbf{H} = \sum_{i=1}^{N} \bar{\mathbf{P}}_c^i \cdot (\bar{\mathbf{P}}_g^i)^T. \tag{25}$$

Note that the position in each coordinate system is 3-dimensional, and $\bar{\mathbf{P}}_g^i$ and $\bar{\mathbf{P}}_c^i$ are each represented by a 3×1 vector. Hence, the $\mathbf{H}$ given by (25) is a 3×3 matrix. We decompose or factorize matrix $\mathbf{H}$ by the SVD method as:

$$[\mathbf{U}, \mathbf{S}, \mathbf{V}] = SVD(\mathbf{H}). \tag{26}$$

Then the optimal rotation $\mathbf{R}_t$ can be derived as:

$$\mathbf{R}_t = \mathbf{V} \cdot \mathbf{U}^T. \tag{27}$$

A special case must be considered here. When the determinant of $\mathbf{V}$ is -1, we must multiply the third column of $\mathbf{R}_t$ by -1 to obtain the correct rotation.

In Step 3, after obtaining the rotation $\mathbf{R}_t$, we can easily derive the translation $\mathbf{T}_t$ by the following equation.

$$\mathbf{T}_t = \mathbf{O}_g - \mathbf{R}_t \cdot \mathbf{O}_c. \tag{28}$$

Thus we derive the orientation $\mathbf{R}_t$ and position $\mathbf{T}_t$ of the UAV in the given global coordinate system.

IV. EXPERIMENTAL STUDY AND DISCUSSIONS

A. EXPERIMENT SETUP

To validate the performance of the RFUAV system, we conduct a set of experiments in a representative indoor environment at the RFID Laboratory of Auburn University, Auburn, AL. To build a prototype of RFUAV, we employ a Zebra FX7500 RFID reader [37] and four Zebra AN720 Antennas [38] to collect observation of the RFID tags. The entire RFID system operates in the 902 $\sim$ 928 MHz band, which is the frequency range allocated by Federal Communications Commission (FCC) in the USA. The Zebra FX7500 reader is one of the most widely used RFID products in the market. It is compatible with EPC Gen2 [39] standard, and provides the Low-Level Reader Protocol (LLRP) through an Ethernet port to report the RFID readings. The reader interrogates the RFID tags and sends query reports that includes the information

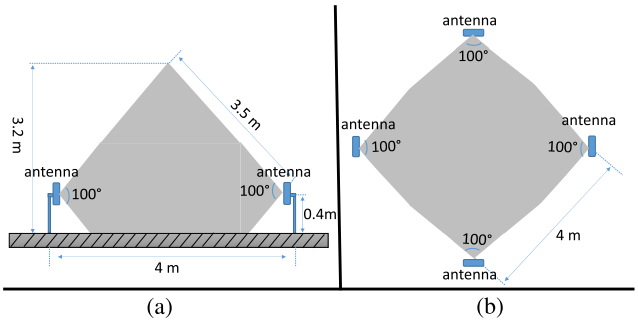

FIGURE 6. Antennas setup for the RFUAV prototype: (a) Side view of the RFID detectable field; (b) Top view of the RFID detectable field.

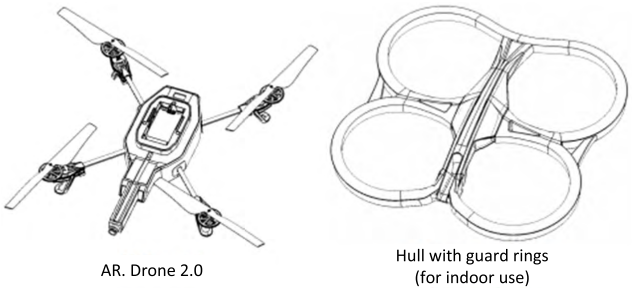

FIGURE 7. Illustration of the Parrot AR. Drone 2.0 schematic.

on EPC, RSSI, phase, time stamp and channel index. The Zebra AN720 Antennas provide a 5.5 $\sim$ 6 dB gain and a left circular polarization with 100° beamwidth. The size of each antenna is $132.8 \times 132.8 \times 18$ mm^3. Each antenna is mounted on a holder of 0.4 m high. The four antennas with their holders are deployed at the corners of a square of 4×4 m^2. During our experiment, the reader is operated at the maximum RF transmission power of about 33 dBm. This allows the reading range of the antenna up to 6 m. Four antennas create a detectable field and can interrogate an RFID tag simultaneously. The configuration of our experiment is shown in Fig. 6.

The Parrot AR Drone2.0 Elite Edition [40], a low-cost platform with good maneuverability, is employed as our indoor UAV platform. It consists of a drone shell, hull, and battery, as shown in Fig. 7. A fully charged battery can support the UAV in continuous flight for 15 minutes. The AR Drone is equipped with a front and bottom camera, a sonar, and an IMU. With readings from these sensors, it can localize itself by a sensor fusion method, such as Parallel Tracking and Mapping (PTAM) [41] that estimates a 3D pose of the UAV in an unknown environment.

Three UHF passive RFID tags are attached to the UAV as illustrated in Fig. 8. Our experimental RFID tag is Smartrac Dogbone - Impinj Monza R6 [42], which is widely used in the retail market. It is equipped with an Impinj Monza R6 chip that provides up to -22.1 dBm read wake-up sensitivity and up to -18.8 dBm write wake-up sensitivity [43]. Our proposed RFUAV is not restricted to any specific tag layout, and a detailed experiment will be presented later to

TABLE 1. Eperiment configuration and parameters.

Parameter	*Value*
RFID reader	Zebra FX7500 RFID reader
Antenna	Zebra AN720 Antennas
Number of antennas	4
Antenna frequency	902 $\sim$ 928 MHz
Antenna gain	5.5 $\sim$ 6.0 dB
Antenna beamwidth	100°
Antenna height	0.4 m
Transmission power	33 dBm
RFID tag	Smartrac Dogbone - Impinj Monza R6
Tag read sensitivity	-22.1 dBm
Tag write sensitivity	-18.8 dBm
UAV	Parrot AR Drone2.0 Elite Edition
UAV battery	15 min
Dynamic ground-truth positioning system	Ultra-Wideband (UWB) positioning system from PLUSLocation.LLC

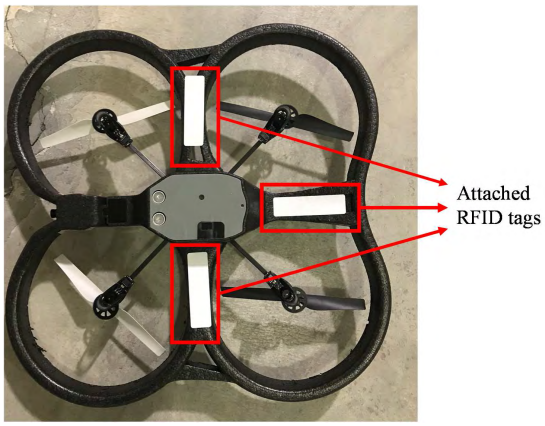

FIGURE 8. The Parrot AR Drone2.0 UAV with three attached RFID tags.

demonstrate the effect of various tag layouts. In our experiments, the Electronic Product Code (EPC) of each tag serves as its identity to consistently and accurately distinguish the received readings from that of other RFID tags. During the experiments, to achieve accurate localization and orientation estimation, the initial position of tags in the three-dimensional global system and the UAV's built-in coordinate system are given. The configuration for the experiments reported in this section is summarized in Table 1.

To precisely collect the ground-truth for the poses and trajectories of the UAV, we design two experimental settings, a confined and a dynamic setup. In the confined setup, the UAV was mounted to an adjustable rolling rack, as illustrated in Fig. 9(a). The UAV-mounted rolling rack is easily maneuverable throughout our experimental field, and the height of the UAV can be adjusted from 0.8m to 1.6m. During the experiments, we manually moved the rolling rack instead

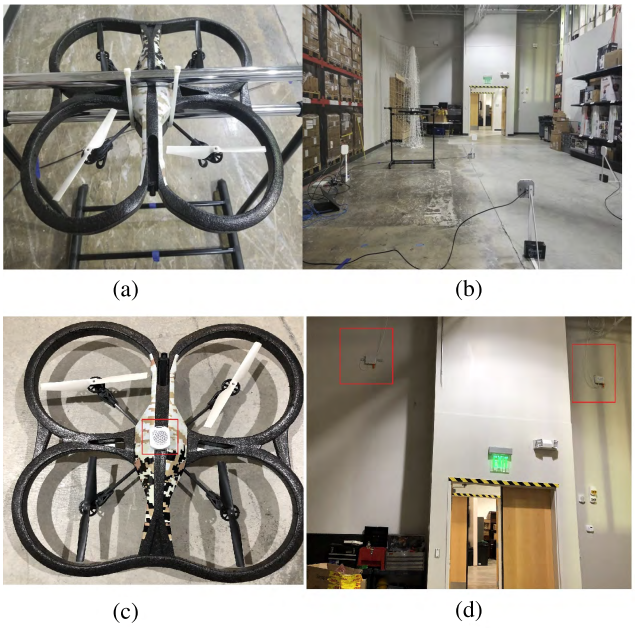

FIGURE 9. (a) UAV carried by a rolling rack in the confined setup, (b) The UAV confined rolling rack moves in the experimental field, (c) An UWB tag is attached to the UAV in dynamic setup, the UWB tag is marked by a red rectangle, (d) Two nodes that are marked in red of the UWB positioning system, there are 6 nodes are installed in the experimental field.

of flying the UAV, as shown in Fig 9(b). In this setting, the ground truth of the moving trajectories can be represented by a set of discrete sample poses, including positions and orientations, which are precisely and manually measured while the rolling rack is at a sampling point. Considering the errors usually introduced by taking measurements manually, these ground truth data can provide sub-centimeter accuracy. However, the confined setup enables us to provide extremely precise ground-truth trajectories and poses in a semi-static manner. To evaluate our RFUAV in a dynamic manner and obtain ground truth while it is flying, we designed the dynamic setup. An Ultra-Wideband (UWB) positioning system from PLUSLocation.LLC [50] was installed to cover the entire space of the RFID Laboratory in the Auburn University campus. We attached a UWB tag to the UAV, which is shown in Fig 9(c), in such a way that while the UAV is flying, its positions can be read by the system in real-time. The localization accuracy of the UWB system in the experimental field was 3cm with a limited area of 4×4 m^2. Although we are able to track the UAV in a dynamic way in this setup, it provides us with position information but no orientation information, so the UAV's position accuracy is compromised. Therefore, we utilized the confined setup for quantitative experiments and the dynamic setup for qualitative experiments or experiments where the UAV must fly.

B. ACCURACY OF RFID TAG TRACKING

We first launched an experiment to evaluate the performance of the RFID tracker of RFUAV by comparing its accuracy with that ofthe state-of-art approach Tagoram [27].

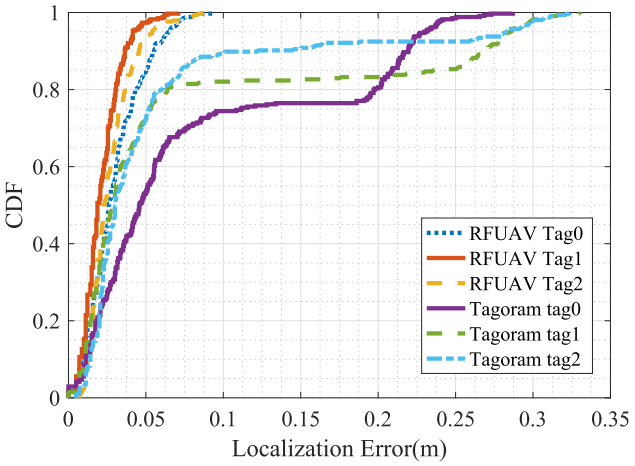

FIGURE 10. CDFs of multiple tags' localization errors for RFUAV and Tagoram.

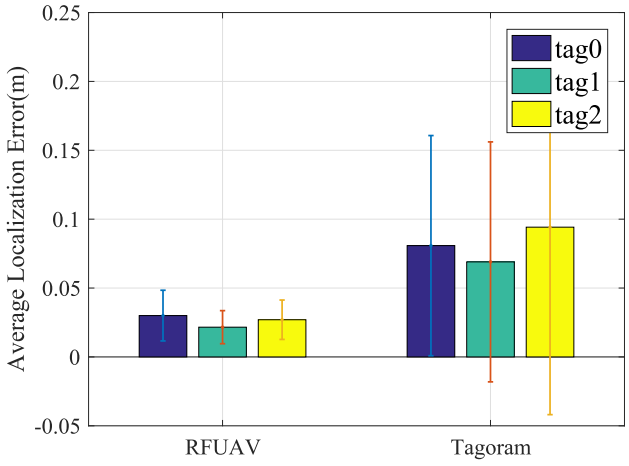

FIGURE 11. Average distance error and standard deviation of RFUAV and Tagoram.

To guarantee the fairness of comparison, the same equipment is utilized for both approaches. The confined setup was used for this experiment and three UHF-passive RFID tags were attached to the UAV. These tags were moved around the experimental field by manually pushing the UAV-mounted rolling rack. The ground-truth positions of each tag were manually measured at the sampling positions of the trajectories. The moving trajectories were unknown to the proposed RFID tracker or to Tagoram. Therefore, the Tagoram functioned in uncontrollable mode where the trajectory function is unknown. Tracker performance was evaluated by assessing the amount of errors between the estimated and ground-truth positions of the sampled points.

The experiment results are presented in Fig. 10 and Fig. 11. As shown in Fig. 10, about 80% of all the localization errors for RFUAV are less than 0.04 m. In addition, the RFUAV maximum location error is 0.085 m, while the maximum error for Tagoram is 0.33 m. Obviously, the proposed RFID tracker of RFUAV is more suitable for a complex indoor environment. Fig. 11 presents the average localization error and standard deviation (see error bars) of RFUAV and Tagoram. The average localization errors of RFUAV are much less than those of Tagoram. Furthermore, the RFUAV's standard deviations are also much smaller, indicating more robust performance by our proposed scheme.

C. ACCURACY OF POSE ESTIMATION

In this section, we investigate the pose accuracy of the RFUAV system by conducting a set of experiments to evaluate the impact of two important system configurations: the layout and number of attached tags on the UAV.

1) EFFECT OF THE LAYOUT OF TAGS

The design of our proposed pose estimator allows for RFUAV to not be restricted by any specific tag layout. To demonstrate this advantage, we attached three tags in four representative layouts, which is illustrated in Fig. 12. In Layout 1

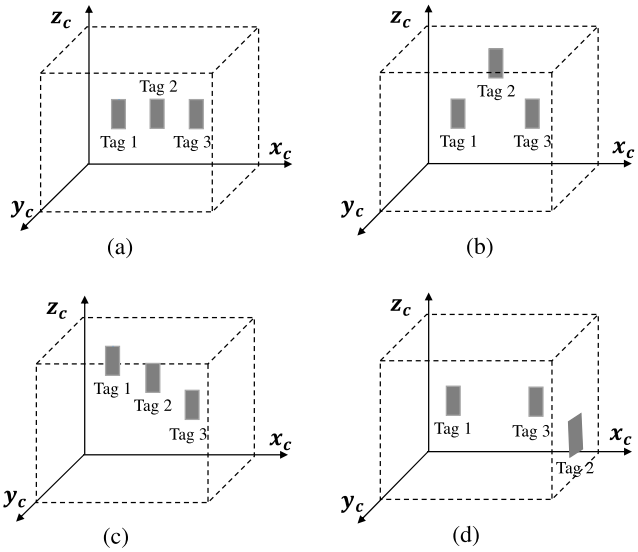

FIGURE 12. Four representative layouts of the attached tags in the UAV's built-in coordinate system: (a) Layout 1; (b) Layout 2; (c) Layout 3; (d) Layout 4.

in Fig. 12(a) shows three tags arranged in a plane with two identical coordinate values against the UAV's built-in coordinate system. In Fig. 12(b), Layout 2 shows three tags arranged in a plane, but not on a straight line. For Layout 3 in Fig. 12(c), three tags are arranged in a plane, but on a straight line. As shown in Fig. 12(d), Layout 4 consists of three tags arranged neither in a plane nor on a straight line. This experiment was conducted in the confined setup, and we moved the UAV-mounted rolling rack throughout the environment in the same small-scale trajectory (with a length of 0.5 m) for each representative tag layout. Each trajectory is sampled in every 2cm, that is 25 points for every trajectory. We compared the pose accuracy for these four layouts, and those results are presented in Fig. 13.

Fig. 13 shows that the average position errors for the four layouts are 0.038 m, 0.016 m, 0.019 m, and 0.019 m, respectively. The average orientation errors for the four layouts are

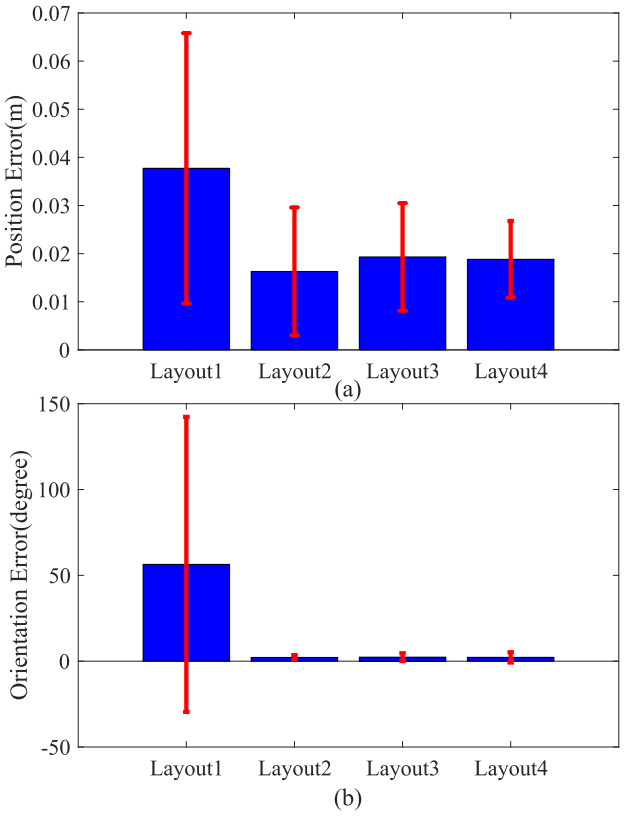

FIGURE 13. (a) Position errors of different layouts of attached RFID tags; (b) Orientation errors of different layouts of attached RFID tags.

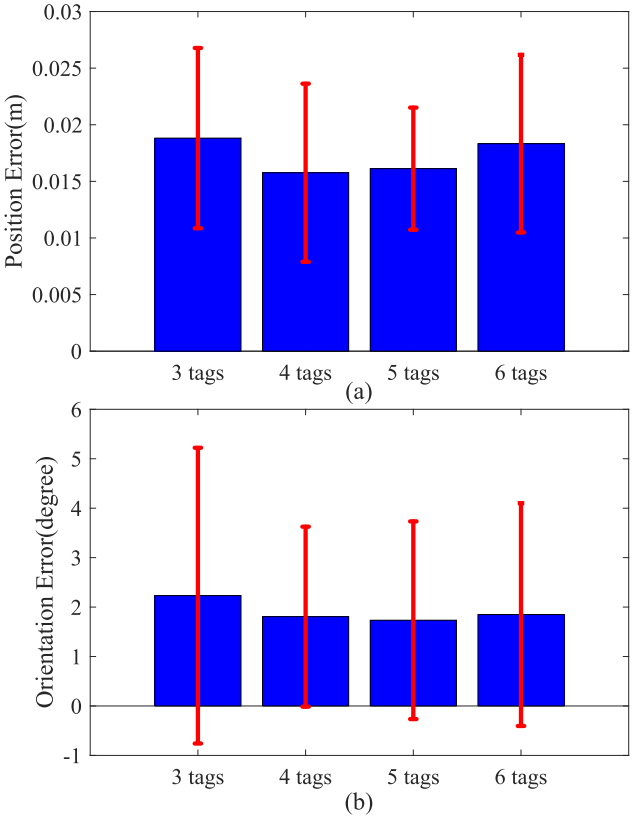

FIGURE 14. (a) Position errors of different numbers of attached RFID tags, (b) Orientation errors of different numbers of attached RFID tags.

56.4°, 2.0°, 2.3°, and 2.2°, respectively. Clearly, all layouts achieve a small error (less than 0.04 m) on positioning of the UAV. However, the orientation of Layout 1 yields a relatively greater error of 56.4°, due to the arrangement of tags being in an extremely adversarial layout; two coordinate values in the UAV's built-in coordinate system are identical. This layout is vulnerable to small turbulence of estimated global tag locations. It may also cause the estimated orientation of the UAV to reverse. However, Fig. 13 shows that except for this extreme case, the other layouts of tags have an orientation error of less than 2.5° and do not affect the performance of RFUAV.

2) EFFECT OF THE NUMBER OF TAGS

The RFUAV requires at least three tags to compute a 6-DoF pose in an indoor environment. We examined the effect of the number of attached tags on pose accuracy. We attached three, four, five, and six tags on the UAV in each experiment. According to the previous experiments, the layout of the tags does not affect the tracking precision (except for the extreme case). Based on the previous experiment and to guarantee a fair comparison in this experiment, Layout 4 is used. Fig. 15 illustrates the experimental layout. For each trial of the experiment, the same trajectory (a confined setup with a length of 0.5 m and 25 sampling points) is followed by the UAV. This experiment's results are presented in Fig. 14.

Fig. 14 presents the relationship between pose error and the number of tags that are used in RFUAV. From Fig. 14(a) we can see that the highest position error, 0.019 m, is achieved when 3 tags are used in our system, while the lowest position error, 0.016 m, is achieved with 4 tags. The variation of the position errors among different sets of tags is less than 3 mm. Fig. 14(b) shows that the number of tags does not affect the orientation accuracy neither. All sets of tags provide a similar orientation error around 2°. Thus, it is safe to say that the RFUAV system does not exhibit an obvious difference in performance when different numbers of tags are deployed. For experiments herein, we attached three tags to the bottom of the UAV's hull, as shown in Fig. 8. Due to the uneven shape of the hull, the deployed layout is Layout 4 in Fig. 12(d), which we have discussed previously.

3) COMPARISON WITH STATE-OF-THE-ART METHOD

Next, we compare our approach to the state-of-the-art UAV indoor localization method. We implement the recently developed Parallel Tracking and Mapping (PTAM) scheme [41] with our Parrot ARDrone 2.0 hardware. The PTAM based implementation utilizes data from a 2D camera, sonar, and an IMU to estimate a 3D pose in an unknown environment. We conducted this first experiment under the confined setup, and each trial followed the same trajectories in our experimental filed. We manually moved the UAV-mounted rolling

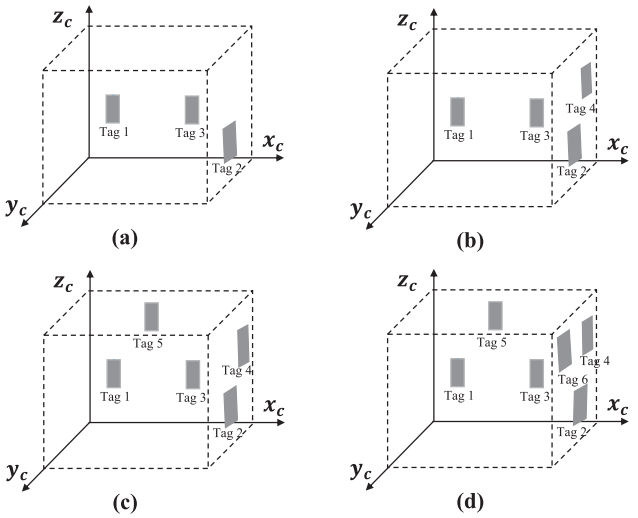

FIGURE 15. Layout 4 is deployed for evaluating the effect of the number of tags on pose accuracy: (a) three tags, (b) four tags, (c) five tags, and (d) six tags.

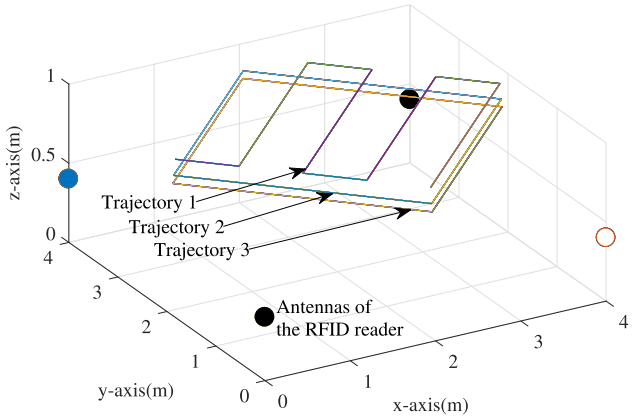

FIGURE 16. Examples of the experimental trajectories.

rack back and forth in 4×4 m^2 field and adjusted the UAV's vertical height to make the total length of the trajectories more than 10 m. An example of the trajectories is shown in Fig 16. The proposed RFUAV system localizes the UAV using readings from the RFID reader, while the PTAM localizes the UAV with multi-modal data fusion from the Parrot ARDrone2.0 platform.

The results of comparing the CDFs of position and orientation error are presented in Fig. 17. As shown in Fig. 17(a), RFUAV achieves a median position error of about 0.04 m, and the 90th percentile error is about 0.06 m. The PTAM system achieves a median error about 0.067 m, and the 90th percentile error is slightly lower than 0.1 m. RFUAV outperforms PTAM with a great reduction of both the median error and 90th percentile error. Fig. 17(b) compares the orientation accuracy of RFUAV and PTAM. It shows that RFUAV can achieve a median error about 2°. On the other hand, PTAM has a median error about 2.5°. Obviously, RFUAV can provide a more reliable orientation estimation than PTAM,

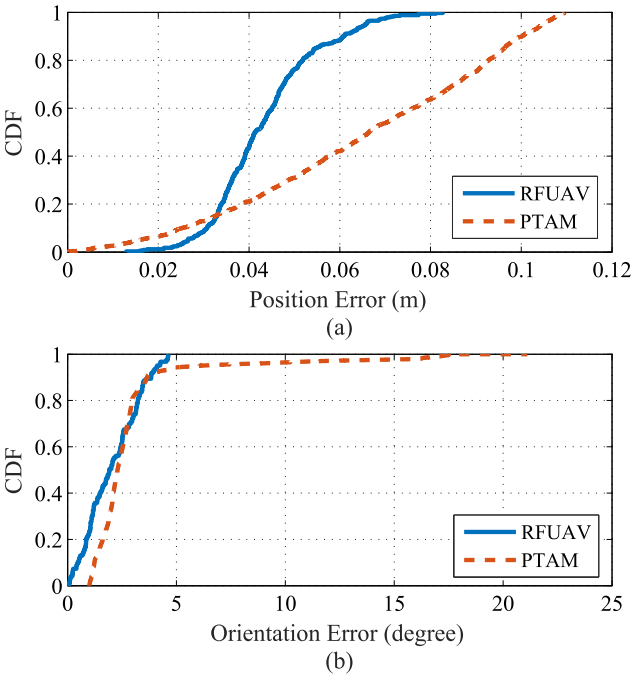

FIGURE 17. Comparison of localization accuracy: (a) CDFs of position errors of RFUAV and PTAM; (b) CDFs of orientation errors of RFUAV and PTAM.

because the maximum orientation error of RFUAV is less than 5°, while the maximum orientation error of PTAM is up to 21°.

Our second experiment was conducted under the dynamic setup to compare the performance of the two methods, while the UAV is hovering in a position in the air. During the experiment, we sealed all air vents in the laboratory to create a windless environment for the UAV. Absolute position oscillations were about 10 cm in each direction of x, y, and z. Usually, vision-based algorithms, such as PTAM, suffer from significant position error when the UAV is hovering due to camera data noise and the slight position shift induced by IMU. For vision-based positioning systems, the current localization result depends on the estimation of its previous location. So the accumulative error will persistently increase as flight time goes on [44], especially, while the UAV is hovering. We compared the position error between RFUAV and PTAM while the UAV hovered in a fixed position for 35 seconds, the results of which are presented in Fig. 18. Results show that the position error of PTAM increases continuously; the error grows to 0.2 m by the end of the 35-second period. Whereas, RFUAV achieves a stable position error while the UAV hovers for the same period of time. The maximum position error of RFUAV is less than 0.08 m. From Fig. 18, we conclude that RFUAV is resilient to accumulative error, and it can provide a precise position for a hovering UAV. RFUAV localizes the UAV at each individual observation from the RFID reader. Even though the measurement noise in the observation will distort the estimated position, the observation model of the RFID does not accumulate error over time.

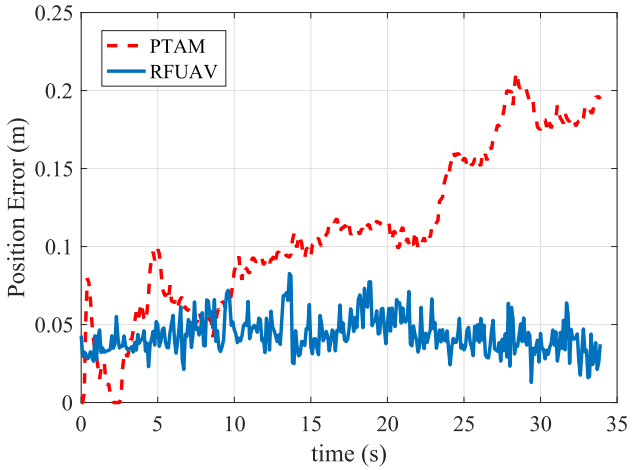

FIGURE 18. Cumulative positioning error of RFUAV and PTAM while the UAV hovers for 35 seconds.

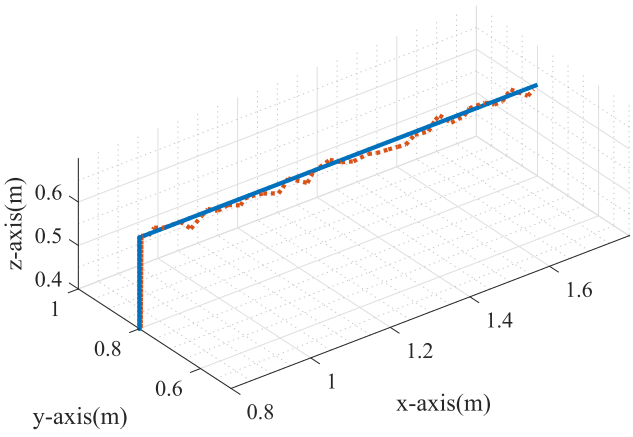

FIGURE 19. The UAV Trajectory as estimated by RFUAV (red dashed line) and ground truth (blue solid line).

4) NAVIGATIONAL TRAJECTORY

To evaluate the RFUAV system's potential for indoor autonomous navigation, we conducted an experiment under the dynamic setup in our indoor laboratory. During the experiment, the UAV moved through a set of fixed destination waypoints. The trajectory of the movement is represented by the positions provided by RFUAV. The experiment's results are shown in Fig. 19, and illustrate that the estimated trajectory is highly accurate, with only a small disturbance around the ground-truth. Thus, control of the UAV becomes quite straightforward with RFUAV. As shown by other works, the pose estimation algorithm plays a critical role in the control strategy of autonomous UAV navigation [45], [46]. Thus, our proposed RFUAV system can greatly improve the performance of autonomous navigation of UAVs in indoor environments.

V. CONCLUSION

In this paper, we proposed an innovative indoor localization system for UAVs, termed RFUAV, which provides precise 6-DoF orientation and location estimation with a COTS RFID reader and tags. A Bayesian filter was leveraged to estimate the location of tags with phase difference. Then, we estimated pose with an SVD-based algorithm. To evaluate the performance of our RFUAV system, we conducted exhaustive experiments in an indoor environment. The results demonstrated that our RFUAV system can achieve an accurate location estimation with a mean error of 0.04 m and an accurate orientation estimation with a mean error of 2.5°. To the best of our knowledge, this was the first feasible UHF passive RFID based localization system for UAVs. RFUAV is a promising method for indoor UAV navigation that is simple, computationally cost-effective, and not dependent on specific UAV architecture.

REFERENCES

[1] K. P. Valavanis, ed., *Advances in Unmanned Aerial Vehicles: State of the Art and the Road to Autonomy*. New York, NY, USA: Springer, 2007.

[2] J. Courbon, Y. Mezouar, N. Guénard, and P. Martinet, "Vision-based navigation of unmanned aerial vehicles," *Control Eng. Pract.*, vol. 18, no. 7, pp. 789–799, Jul. 2010.

[3] B. Hérissé, T. Hamel, R. Mahony, and F.-X. Russotto, "A terrain-following control approach for a VTOL unmanned aerial vehicle using average optical flow," *Auton. Robots*, vol. 29, nos. 3–4, pp. 381–399, 2010.

[4] S. Klose, J. Wang, M. Achtelik, G. Panin, F. Holzapfel, and A. Knoll, "Markerless, vision-assisted flight control of a quadrocopter," in *Proc. IEEE/RSJ Int. Conf. Intell. Robots Syst.*, Taipei, Taiwan, Oct. 2010, pp. 5712–5717.

[5] K. Celik, S.-J. Chung, M. Clausman, and A. K. Somani, "Monocular vision SLAM for indoor aerial vehicles," in *Proc. IEEE/RSJ Int. Conf. Intell. Robots Syst.*, St. Louis, MI, USA, Oct. 2009, pp. 1566–1573.

[6] J. Engel, J. Sturm, and D. Cremers, "Camera-based navigation of a low-cost quadrocopter," in *Proc. IEEE/RSJ Int. Conf. Intell. Robots Syst.*, Vilamoura, Portugal, Oct. 2012, pp. 2815–2821.

[7] A. Chiuso, P. Favaro, H. Jin, and S. Soatto, "Structure from motion causally integrated over time," *IEEE Trans. Pattern Anal. Mach. Intell.*, vol. 24, no. 4, pp. 523–535, Apr. 2002.

[8] A. Noureldin, T. B. Karamat, M. D. Eberts, and A. El-Shafie, "Performance enhancement of MEMS-based INS/GPS integration for low-cost navigation applications," *IEEE Trans. Veh. Technol.*, vol. 58, no. 3, pp. 1077–1096, Mar. 2009.

[9] K. Pahlavan, X. Li, and J.-P. Mäkelä, "Indoor geolocation science and technology," *IEEE Commun. Mag.*, vol. 40, no. 2, pp. 112–118, Feb. 2002.

[10] J. Xiao, Z. Zhou, Y. Yi, and L. M. Ni, "A survey on wireless indoor localization from the device perspective," *ACM Comput. Surv.*, vol. 49, no. 2, Nov. 2016, Art. no. 25.

[11] M. Kotaru, K. Joshi, D. Bharadia, and S. Katti, "SpotFi: Decimeter level localization using WiFi," in *Proc. ACM SIGCOMM*, London, U.K., Aug. 2015, pp. 269–282.

[12] X. Wang, L. Gao, and S. Mao, "CSI phase fingerprinting for indoor localization with a deep learning approach," *IEEE Internet Things J.*, vol. 3, no. 6, pp. 1113–1123, Dec. 2016.

[13] X. Wang, L. Gao, and S. Mao, "BiLoc: Bi-modal deep learning for indoor localization with commodity 5GHz WiFi," *IEEE Access*, vol. 5, no. 1, pp. 4209–4220, Mar. 2017.

[14] X. Wang, X. Wang, and S. Mao, "ResLoc: Deep residual sharing learning for indoor localization with CSI tensors," in *Proc. IEEE PIMRC*, Montreal, QC, Canada, Oct. 2017, pp. 1–6.

[15] X. Wang, L. Gao, S. Mao, and S. Pandey, "CSI-based fingerprinting for indoor localization: A deep learning approach," *IEEE Trans. Veh. Technol.*, vol. 66, no. 1, pp. 763–776, Jan. 2017.

[16] J. Xiong and K. Jamieson, "ArrayTrack: A fine-grained indoor location system," in *Proc. USENIX NSDI*, Lombard, IL, USA, Apr. 2013, pp. 71–84.

[17] J. Wang, D. Vasisht, and D. Katabi, "RF-IDraw: Virtual touch screen in the air using RF signals," in *Proc. ACM SIGCOMM*, Chicago, IL, USA, Aug. 2014, pp. 235–246.

[18] L. Shangguan, Z. Yang, A. X. Liu, Z. Zhou, and Y. Liu, "Relative localization of RFID tags using spatial-temporal phase profiling," in *Proc. USENIX NSDI*, Oakland, CA, USA, May 2015, pp. 251–263.
[19] S. Pradhan, E. Chai, K. Sundaresan, L. Qiu, M. A. Khojastepour, and S. Rangarajan, "RIO: A pervasive RFID-based touch gesture interface," in *Proc. ACM MobiCom*, Snowbird, UT, USA, Oct. 2017, pp. 261–274.
[20] B. R. Stojkoska, J. Palikrushev, K. Trivodaliev, and S. Kalajdziski, "Indoor localization of unmanned aerial vehicles based on RSSI," in *Proc. IEEE EUROCON*, Ohrid, Macedonia, Jul. 2017, pp. 120–125.
[21] J. Tiemann, F. Schweikowski, and C. Wietfeld, "Design of an UWB indoor-positioning system for UAV navigation in GNSS-denied environments," in *Proc. Int. Conf. Indoor Positioning Indoor Navigat.*, Banff, AB, Canada, Oct. 2015, pp. 1–7.
[22] K. Li, C. Wang, S. Huang, G. Liang, X. Wu, and Y. Liao, "Self-positioning for UAV indoor navigation based on 3D laser scanner, UWB and INS," in *Proc. IEEE ICIA*, Ningbo, China, Aug. 2016, pp. 498–503.
[23] B. Hardgrave, "Try it you'll like it!-The RFID lab's annual state-of-adoption report of US retailers," *RFID J.*, Aug. 2015. Accessed: Dec. 31, 2018. [Online]. Available: http://www.rfidjournal.com/articles/view?13454
[24] J. Zhang, Y. Lyu, J. Patton, S. C. G. Periaswamy, and T. Roppel "BFVP: A probabilistic UHF RFID tag localization algorithm using Bayesian filter and a variable power RFID model," *IEEE Trans. Ind. Electron.*, vol. 65, no. 10, pp. 8250–8259, Oct. 2018.
[25] Z. Yanjun, "Survivable RFID systems: Issues, challenges, and techniques," *IEEE Trans. Syst., Man, Cybern. C, Appl. Rev.*, vol. 40, no. 4, pp. 406–418, Jul. 2010.
[26] S. Azzouzi, M. Cremer, U. Dettmar, R. Kronberger, and T. Knie, "New measurement results for the localization of UHF RFID transponders using an Angle of Arrival (AoA) approach," in *Proc. IEEE RFID*, Orlando, FL, USA, Apr. 2011, pp. 91–97.
[27] L. Yang, Y. Chen, X. Li, C. Xiao, M. Li, and Y. Liu, "Tagoram: Real-time tracking of mobile RFID tags to millimeter-level accuracy using COTS devices," in *Proc. ACM MobiCom*, Maui, HI, USA, Sep. 2014, pp. 237–248.
[28] F. Gandino, B. Montrucchio, M. Rebaudengo, and E. R. Sanchez, "On improving automation by integrating RFID in the traceability management of the agri-food sector," *IEEE Trans. Ind. Electron.*, vol. 56, no. 7, pp. 2357–2365, Jul. 2009.
[29] J. S. Choi, B. R. Son, H. K. Kang, and D. H. Lee, "Indoor localization of unmanned aerial vehicle based on passive UHF RFID systems," in *Proc. IEEE URAI*, Daejeon, South Korea, Nov. 2012, pp. 188–189.
[30] Y. Bu, L. Xie, J. Liu, B. He, Y. Gong, and S. Lu, "3-dimensional reconstruction on tagged packages via RFID systems," in *Proc. IEEE SECON*, San Diego, CA, USA, Jun. 2017, pp. 1–9.
[31] T. Wei and X. Zhang, "Gyro in the air: Tracking 3D orientation of battery-less Internet-of-Things," in *Proc. ACM MobiCom*, New York, NY, USA, Oct. 2016, pp. 55–68.
[32] Q. Lin, L. Yang, Y. Sun, T. Liu, X.-Y. Li, and Y. Liu, "Beyond one-dollar mouse: A battery-free device for 3D human-computer interaction via RFID tags," in *Proc. IEEE INFOCOM*, Hong Kong, Apr./May 2015, pp. 1661–1669.
[33] Z. Kaleem and M. H. Rehmani, "Amateur drone monitoring: State-of-the-art architectures, key enabling technologies, and future research directions," *IEEE Wireless Commun.*, vol. 25, no. 2, pp. 150–159, Apr. 2018.
[34] M. Z. Anwar, Z. Kaleem, and A. Jamalipour, "Machine learning inspired sound-based amateur drone detection for public safety applications," *IEEE Trans. Veh. Technol.*, vol. 68, no. 3, pp. 2526–2534, Mar. 2019.
[35] S. Thrun, W. Burgard, and D. Fox, *Probabilistic Robotics*. Boston, MA, USA: MIT Press, 2005.
[36] *Impinj*. Accessed: Dec. 31, 2018. [Online]. Available: http://www.impinj.com/
[37] Zebra. *FX7500*. Accessed: Dec. 31, 2018. [Online]. Available: https://www.zebra.com/us/en/products/rfid/rfid-readers/fx7500.html
[38] Zebra. *AN720*. Accessed: Dec. 31, 2018. [Online]. Available: https://www.zebra.com/us/en/products/rfid/rfid-reader-antennas/an720.html
[39] *GS1 US*. Accessed: Dec. 31, 2018. [Online]. Available: https://www.gs1us.org/
[40] *Parrot ARDrone2.0*. Accessed: Dec. 31, 2018. [Online]. Available: https://www.parrot.com/global/drones/parrot-ardrone-20-elite-edition#parrot-ardrone-20-elite-edition
[41] G. Klein and D. Murray, "Parallel tracking and mapping for small AR workspaces," in *Proc. IEEE/ACM ISMAR*, Nara, Japan, Nov. 2007, pp. 225–234.
[42] Samrtarc, Dogbone. Accessed: Dec. 31, 2018. [Online]. Available: https://www.smartracgroup.com/files/content/Products_Services/PDF/0028_SMARTRAC_DOGBONE.pdf
[43] Impinj, R6. *Monza R6 Product Brief / Datasheet*. Accessed: Dec. 31, 2018. [Online]. Available: https://support.impinj.com/hc/en-us/articles/202765328-%20MonzaR6ProductDatasheet
[44] Y. Chen, R. Huang, and Y. Zhu, "A cumulative error suppression method for UAV visual positioning system based on historical visiting information," *Eng. Lett.*, vol. 25, no. 4, pp. 1–7, Nov. 2017.
[45] A. S. Huang, A. Bachrach, P. Henry, M. Krainin, D. Maturana, D. Fox, and N. Roy, "Visual odometry and mapping for autonomous flight using an RGB-D camera," in *Robotics Research*, H. Christensen and O. Khatib, Eds. Cham, Switzerland: Springer, 2017, pp. 235–252.
[46] C. Teulière, L. Eck, E. Marchand, and N. Guénard, "3D model-based tracking for UAV position control," in *Proc. IEEE/RSJ IROS*, Taipei, Taiwan, Oct. 2010, pp. 1084–1089.
[47] S. Umeyama, "Least-squares estimation of transformation parameters between two point patterns," *IEEE Trans. Pattern Anal. Mach. Intell.*, vol. 13, no. 4, pp. 376–380, Apr. 1991.
[48] D. W. Eggert, A. Lorusso, and R. B. Fisher, "Estimating 3-D rigid body transformations: A comparison of four major algorithms," *Mach. Vis. Appl.*, vol. 9, nos. 5–6, pp. 272–290, 1997.
[49] S. Chen and K. C. Ho, "Accurate localization of a rigid body using multiple sensors and landmarks," *IEEE Trans. Signal Process.*, vol. 63, no. 24, pp. 6459–6472, Dec. 2015.
[50] Pluslocation, LLC. *Enabling Innovative Location Services*. Accessed: Dec. 31, 2018. [Online]. Available: https://pluslocation.com/

JIAN ZHANG received the B.Sc. and M.Sc. degrees in applied physics from Sichuan University, Chengdu, China, in 2001 and 2008, respectively, and the Ph.D. degree in the electrical and computer engineering from Auburn University, Auburn, AL, USA, in 2016, where he is currently a Postdoctoral Research Fellow with the RFID Lab. His work has focused on improving the efficiency of supply chain management for the industry and the business. His research interests include RFID technologies and applications, the Internet of Things, indoor localization, UAV, and collaborative robotics.

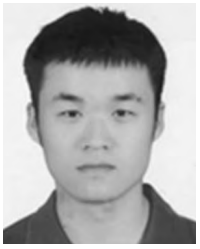

XIANGYU WANG received the B.S. degree in electrical engineering from the Taiyuan Institute of Technology, Taiyuan, China, in 2014, and the M.S. degree in electrical and computer engineering from Auburn University, Auburn, AL, USA, in 2017, where he is currently pursuing the Ph.D. degree in ECE. His research interests include machine learning, indoor localization, and IoT. He was a co-recipient of the Best Student Paper Award of the IEEE PIMRC 2017.

ZHITAO YU received the B.S. degree in electrical engineering from the Nanjing University of Posts and Telecommunication, Nanjing, China, in 2016, and the M.S. degree in electrical and computer engineering from Auburn University, Auburn, AL, USA, in 2018, where he is currently pursuing the Ph.D. degree in ECE. His research interests include indoor localization, deep learning, and UAV indoor navigation.

YIBO LYU was born in Shenyang, China. He received the bachelor's degree in control science and engineering from Zhejiang University, in 2009, and the Ph.D. degree in electrical and computer engineering from Auburn University, in 2018, where he is currently pursuing the Ph.D. degree with the Electrical and Computer Engineering Department. His research interests include robotics, SLAM, RFID, and UAV. His research was sponsored by RFID Lab, Auburn University.

SHIWEN MAO (S'99–M'04–SM'09–F'19) received the Ph.D. degree in electrical and computer engineering from Polytechnic University, Brooklyn, NY, USA. He was the McWane Associate Professor of electrical and computer engineering with Auburn University, Auburn, AL, USA, from 2012 to 2015, where he is currently the Samuel Ginn Distinguished Professor, and the Director of the Wireless Engineering Research and Education Center (WEREC). His research interests include wireless networks, multimedia communications, and smart grid. He is a Distinguished Speaker from 2018 to 2021. He is on the Editorial Board of the IEEE TRANSACTIONS ON NETWORK SCIENCE AND ENGINEERING, the IEEE TRANSACTIONS ON MOBILE COMPUTING, the IEEE TRANSACTIONS ON MULTIMEDIA, the IEEE INTERNET OF THINGS JOURNAL, the IEEE MULTIMEDIA, the IEEE NETWORKING LETTERS, and ACM GetMobile. Dr. Mao was a recipient of the IEEE ComSoc TC-CSR Distinguished Technical Achievement Award in 2019, the Auburn University Creative Research and Scholarship Award in 2018, several service awards from IEEE ComSoc in 2019, 2017, 2015, and 2013, and the NSF CAREER Award in 2010. He was a co-recipient of the IEEE ComSoc MMTC Best Journal Paper Award in 2019, the IEEE ComSoc MMTC Best Conference Paper Award in 2018, the Best Demo Award from the IEEE SECON 2017, the Best Paper Awards from IEEE GLOBECOM 2016 and 2015, the IEEE WCNC 2015, and the IEEE ICC 2013, and the 2004 IEEE Communications Society Leonard G. Abraham Prize in the Field of Communications Systems.

SENTHILKUMAR CG PERIASWAMY received the Ph.D. degree in computer science from the University of Arkansas, Fayetteville, in 2010. He is currently the Director of Technology for the RFID Lab, Auburn University, a unique collaboration platform that involves end users, suppliers, technology providers, standards organizations, industry groups, and academic institutions on a global scale. He has researched, advised, and executed projects that are enabling efficient adoption of RFID and sensor fusion in retailing, aerospace, manufacturing, and transportation. His research interests include common goal of making the adaptation of RFID and related sensor technologies more secure, efficient, reliable and useful.

JUSTIN PATTON is the Director with the RFID Lab, Auburn University, a research institute focusing on the business case and technical implementation of emerging technologies in retail, supply chain, aerospace, and manufacturing. The RFID Lab is a unique private/academic partnership between users, technology vendors, standards organizations, and faculty. He has participated in business case research for advanced technology with Walmart, Target, Amazon, FedEx, Dillard's, Macy's, Delta Air Lines, and Boeing. He is currently a researcher for upstream supply chain benefits of RFID in both retail and manufacturing. He is one of the primary developers of the ARC program, the first and most widely utilized international performance validation system for RFID, and is currently working to help standardize the process of testing and certifying RFID performance in all aspects of the supply chain.

XUYU WANG (S'13) received the B.S. degree in electronic information engineering and the M.S. degree in signal and information processing from Xidian University, Xi'an, China, in 2009 and 2012, respectively, and the Ph.D. degree in electrical and computer engineering from Auburn University, Auburn, AL, USA, in 2018. He is an Assistant Professor with the Department of Computer Science, California State University, Sacramento, CA, USA. His research interests include indoor localization, deep learning, and big data. He received a Woltolsz Fellowship at Auburn University. He was a co-recipient of the Second Prize of Natural Scientific Award of Ministry of Education, China, in 2013, the Best Demo Award of IEEE SECON 2017, and the Best Student Paper Award of IEEE PIMRC 2017.